International Journal of Greenhouse Gas Control 125 (2023) 103876

Contents lists available at ScienceDirect

International Journal of Greenhouse Gas Control

journal homepage: www.elsevier.com/locate/ijggc

Sustainable microcrystalline cellulose-based activated carbons for a greener carbon capture at post-combustion conditions

Simba Biti [a], Alan Mccue [b], Davide Dionisi [a], Inês Graça [a], Claudia Fernández Martín [*,a,c]

[a] School of Engineering, Chemical Processes and Materials Engineering Group, University of Aberdeen, Aberdeen AB24 3UE, UK
[b] Department of Chemistry, University of Aberdeen, AB24 3UE
[c] Centre for Energy Transition, University of Aberdeen, United Kingdom

A B S T R A C T

Using lignocellulosic biomass-based sorbents for CO_2 capture potentially offers a sustainable solution to combatting global warming effects and preserving the environment through reduction of greenhouse gas emissions, mainly carbon dioxide. In this work, activated carbons were produced from microcrystalline cellulose using a simple, moderate physical activation procedure. Activations produced at 10, 20 and 30% burn-off along with the original biochar were characterised for their physical and chemical properties, and ability to capture CO_2 by adsorption. CO_2 isotherms showed that the produced activated carbon with a burn-off of 30 wt% produced the highest CO_2 adsorption capacity (2.15 mmol/g at 25°C and 101.3 kPa). Isosteric heats of adsorption of all sorbents ranged from 38.4 to 45.2 kJ/mol, which indicates that strong bonding is present on the surface of the developed sorbents. The highest CO_2 adsorption capacity (1.59 mmol/g at 25°C and 101.3 kPa) under dynamic adsorption conditions at was also exhibited by the sorbent with 30 wt% burn-off. This sample also showed a total CO_2 adsorption capacity of 15.8 mmol/g over 10 adsorption/desorption cycles and similar adsorption-desorption behaviour to that of commercial sorbent Norit R2030CO2 over 10 cycles, at the conditions tested. Additionally, all sorbents maintained a stable CO_2 capture capacity over 10 adsorption-desorption cycles. The results obtained are encouraging for the further development of microcrystalline cellulose-based activated carbons for CO_2 capture.

1. Introduction

Critical to the current industrial revolution is the need for sustainable and environmentally friendly practices. Various reports by the IPCC in the previous decade have emphasised this need whilst highlighting the currently high susceptibility of the environment to the detrimental effects of accelerated climate change (Masson-Delmotte et al., 2021). The 6th assessment report conducted by the IPCC indicated that atmospheric CO_2 concentrations are at their highest level in the last 800,000 years whilst global surface temperatures since 1970 have increased faster than in any other 50-year period within the last 2000 years (Masson-Delmotte et al., 2021). Such an occurrence has been strongly linked to human activity (Masson-Delmotte et al., 2021). Key impacts highlighted by the report include global arctic ice levels being at their lowest since the year 1850 and a higher frequency of both land and marine heatwaves within the last century. The report also forecasts that without substantial reductions to CO_2 emissions along with other greenhouse gas emissions, global surface temperatures since the period 1850-1900 will exceed 2°C warming, which is considered to lead to further severe climatic consequences globally (Masson-Delmotte et al., 2021). Forecasts from this report also indicate that even the Paris Agreement target of 1.5°C is likely to be exceeded. According to this evidence, priority needs to be placed on establishing and soon implementing suitable means to preserve the overall wellbeing of the planet. Part of achieving this objective involves developing industrial practices that mitigate greenhouse gas emissions. To date, this has been evident with the introduction of renewable technologies in favour of fossil-fuel processes to minimise greenhouse gas (GHGs) emissions and clean fuel sources such as green hydrogen and nuclear energy. Such technologies will indeed be beneficial in the long-term, however, as of now, many of these technologies (i.e., green hydrogen) remain nascent in their commercial/industrial-scale development. There exists a more immediate need to cut emissions substantially within this century, such as the year 2050 deadline highlighted in the Paris Agreement (Masson-Delmotte et al., 2021). Carbon Capture, Utilisation and Storage (CCUS) has been identified as a solution that can satisfy the time constraints of current GHG-mitigation targets (Greig and Uden, 2021). CCUS also offers the opportunity to leverage further time to establish /develop other renewable/clean energy technologies (Greig and Uden, 2021). CCUS, however, is not necessarily a solely transitional technology, with development and promise of Bioenergy with Carbon Capture (BECCS) being an example of CCUS remaining valuable in renewable energy

* Corresponding author.
E-mail address: cfmartin@abdn.ac.uk (C.F. Martín).

https://doi.org/10.1016/j.ijggc.2023.103876
Received 13 January 2023; Received in revised form 28 February 2023; Accepted 22 March 2023
Available online 28 March 2023

scenarios (García-Freites et al., 2021). At the moment, post-combustion carbon capture from fossil-fuel emission processes is regarded as the CO_2 capture technology with the most near-term promise (Mukherjee et al., 2019).

Post combustion CO_2 capture processes are generally operated by swing adsorption. Swing adsorption encompasses a cyclic process in which the adsorbate (CO_2), is captured before undergoing removal by desorption or 'regeneration', thus readying the capturing material for another cycle of adsorption/desorption (Mukherjee et al., 2019), (Raganati et al., 2020). Swing adsorption has been developed into three primary methods, namely Pressure Swing adsorption (PSA), Temperature Swing Adsorption (TSA) and Vacuum Swing adsorption (VSA) (Hedin et al., 2013). PSA and VSA are similar in principle as both processes achieve sorbent regeneration through pressure changes. In PSA, the flue gas is fed at high pressure to an adsorption column where CO_2 is selectively adsorbed, before undergoing desorption through reduction of the partial pressures of the adsorbed CO_2 within the column (Raganati et al., 2021). Whilst this process is effective in achieving a regeneration stage with fast desorption kinetics, since adsorption occurs at high pressures, a stage of compression of the flue gases fed to the adsorption column is required, which can substantially hinder the energy feasibility of the process (Raganati et al., 2021). In VSA, adsorption occurs instead at atmospheric pressure and CO_2 is desorbed from the sorbent through the application of a vacuum (Chao et al., 2021). Whilst eliminating the need for compression, VSA is criticised for producing low levels of CO_2 recovery and purity, and likely requires a two-stage process to guarantee high CO_2 recovery and purity (Raganati et al., 2021). In TSA, the CO_2 captured in the material is desorbed by applying a purging gas and heating to temperatures substantially above the temperature used for CO_2 capture (Raganati et al., 2021). However, the use of a purging gas can lead to desorbed CO_2 in diluted streams, which is undesirable for further transportation and storage of the CO_2 (Ammendola et al., 2017).

When considering these processes, whilst PSA and VSA have shown promise for promoting effective regeneration of materials and thus suitable cyclic CO_2 capture, TSA is viewed as the most feasible option, since additional process stages (and thus energy input) are not necessarily required for achieving appropriate high-pressure feed or CO_2 purity/recovery conditions (Raganati et al., 2021), (Zhao et al., 2019). Furthermore, there also exists the potential to retrofit TSA into industrial processes where excess or waste energy is available as a heating source (Chao et al., 2021), thus providing an opportunity to improve the sustainability of the process.

Current CO_2 capture methods in commercial CCUS processes use liquid amine group-containing solvents for capture of CO_2 from post-combustion emissions. Whilst established at a commercial level, key drawbacks associated with amine capture exist and include the consumption of substantial quantities of energy during regeneration, a tendency to degrade equipment rapidly and environmental hazardousness during disposal (Rashidi and Yusup, 2016). Solid porous sorbents such as activated carbons (ACs), are considered advantageous alternatives to liquid amine solvents because of their typically lower energy regeneration requirement, lower capital costs (Rashidi and Yusup, 2016) and ability to adsorb CO_2 over wider temperature and pressure ranges (Heidari et al., 2014). Such advantages are why the use of ACs for CO_2 capture is of major interest, with many studies investigating the prospect of ACs derived from lignocellulosic biomass (LCB), a renewable feedstock available in many waste forms. LCB feedstocks that have been investigated for CO_2 capture include oil palm empty fruit bunch (Joseph et al., 2017), vine shoots (Manyà et al., 2018), waste sugar cane bagasse (Guo et al., 2020), eucalyptus wood (Heidari et al., 2014) and waste tobacco (Sha et al., 2015) amongst others. The use of a lignocellulosic feedstock from waste sources offers the opportunity to add a greater degree of sustainability to CCUS and the lifecycle of a lignocellulosic product if its undesirable waste can be converted into a valuable sorbent product used for another application (Abuelnoor et al., 2021). Cellulose, the primary constituent of LCB is considered the most abundant raw material worldwide with annual global production estimated in the range of 100 billion to 1 trillion tons (Suhas et al., 2016). Cellulose itself has been adopted for various uses in industry such as a binder in pharmaceutical ingredients, a stabiliser or anti-caking agent in food and beverages and a fat substitute or thickener in the cosmetics industry (Trache et al., 2016).

Microcrystalline cellulose (MCC) is of growing interest as a renewable feedstock for various commercial applications because it possesses attractive mechanical properties such as high strength and stiffness, non-toxicity, insolubility in water and high biodegradability (Trache et al., 2014). Subsequent to this interest, various studies and experimental research have been invested in the development of MCC through various isolation techniques and from various sources (Guo et al., 2020). More notably, MCC is proven to be obtainable from various lignocellulosic waste sources including cotton waste, cereal straw, maize cobs, oil palm residues and hemp stalk, thus its obtaining and use from such sources is of benefit to the circular economy (Guo et al., 2020). Whilst lignocellulosic feedstocks such as those previously mentioned could be used in their form for AC production, the access of these feedstocks individually are more limited by their geographical prevalence. Considering the abundance of cellulose, and the abundance of MCC in various waste forms, MCC is a feedstock with greater global accessibility, which is more appropriate to the global challenge of the need for sustainable sorbent production for post combustion capture. As mentioned earlier, the potential of MCC is of substantial interest, including in sorbent applications, such as for the removal of heavy metals and dyes (Garba et al., 2020). However, there lacks experimental investigation of MCC in carbon capture applications, where its physical characteristics could be of appreciable value. Considering the potential of some of the source materials of MCC such oil palm waste, it is worth investigating whether potential exists for the development of MCC-based sorbents for post-combustion carbon capture.

A sorbent that can be considered suitable for post-combustion capture will possess qualities such as high CO_2 adsorption capacity, good selectivity for CO_2 over N_2, ease of regeneration and reusability (Creamer and Gao, 2016). Producing an AC of substantial CO_2 adsorption capacity and selectivity over N_2 is linked to its textural properties, where favourable CO_2 adsorption can be achieved if the AC possesses a high specific surface area and more importantly a substantial presence of micropores ($d < 2$nm) and ultramicropores ($d < 0.7$nm) (Manyà et al., 2018). A parameter such as the isosteric heat of adsorption, whilst a measure that will indicate the strength of affinity between the CO_2 molecule and adsorption site of the AC, will also provide insight into the energy requirement for regeneration, hence a low or moderate heat of adsorption is desirable for ACs that are purposed for CO_2 capture (Manyà et al., 2018). Ease of regeneration and reusability of the material will also be linked to the structural stability of the AC, which will be tested as the AC is subjected to the feeding of gas flows and temperatures elevated from ambient conditions during regeneration (Sethia and Sayari, 2015) often in repeated cycles, as is the case with post combustion capture.

The production of ACs for CO_2 capture is typically achieved either by using physical agents such as steam or CO_2, or chemical agents such as KOH, NaOH or H_3PO4 (Manyà et al., 2018). Both chemical and physical activation methods have been explored in the production of cellulose based ACs. Rehman et al. (Rehman et al., 2021) produced cellulose based ACs for CO_2 capture by a one-step KOH chemical activation with thiourea or urea modification and reported a maximum CO_2 uptake of 6.75 mmol/g at 0°C and 4.40 mmol/g at 25°C (atmospheric pressure) (Suhas et al., 2016). Xu *et al* (Xu et al., 2018) produced ACs for CO_2 capture from Cladophora cellulose by using a one-step, physical activation method with CO_2 as the activating agent. These ACs showed CO_2 uptakes of 5.52 mmol/g at 0°C[19] (atmospheric pressure).

Chemical activation tends to be the preferred method of activation as it typically produces ACs with superior capture capacity. In addition to its use with cellulose-derived ACs, there exists an extensive array of

studies in literature demonstrating the capability of AC production methods encompassing the use of chemical agents, particularly KOH (Rashidi and Yusup, 2016), (Malini et al., 2023). Whilst the effectiveness of an AC production method is important, it is important to envision its use beyond laboratory scale and consider the practicality of employing such larger scales for industrial-scale combustion capture. A key drawback associated with chemical activation is with the chemical agents used possessing corrosive or toxic characteristics. These characteristics create the additional challenge of guaranteeing safe disposal of these activating agents and their by-production after their use (Ahmed et al., 2019). This environmental challenge also extends to procedures that attempt to enhance the CO_2 adsorption capacity of ACs by doping the ACs with nitrogen-rich sources such as ammonia or with some metal oxides such as copper oxide (Malini et al., 2023). Using these agents in large scale sorbent production would ultimately serve as a contradiction to one of the justifications of using physical sorbents over liquid amine solvents, that being their greater environmental friendliness in disposal. This environmental challenge can be avoided with the use of conventional physical activation procedures. In addition, slow pyrolysis, the principal experimental procedure used in producing physically activated ACs, is a commercially ready technology. Various life cycle assessments and feasibility analyses exist in literature in which it is demonstrated that the slow pyrolysis of lignocellulosic feedstock to biochar at a commercial scale offers the potential to generate net positive energy production, in addition to negative carbon emissions (Cheng et al., 2020), (Azzi et al., 2019). Hence the use of physical activation in sorbent production offers a currently more environmentally friendly option at a commercial level, with a greater guarantee of scalability.

During physical activation, these agents will be fed to the sample, diffusing into the surface and pores of the biochar to further enhance the preliminary textural properties developed after carbonisation. As these agents react with the carbonaceous structures within the biochar, additional gaseous products are formed. The reaction mechanisms for these gaseous products are detailed in Equations 1.1 and 1.2 as follows (Rashidi and Yusup, 2016):

CO_2:

$$C(s) + CO_2(g) \rightarrow 2CO(g) \quad (1.1)$$

Steam:

$$C(s) + H_2O(g) \rightarrow CO(g) + H_2(g) \quad (1.2)$$

Regarding physical activating agents, steam is more reactive than CO_2 due to its smaller molecular size which encourages further rapid diffusion into pore structures during activation (Rashidi and Yusup, 2016). This enhanced diffusion leads to the widening of micropores during activation into mesopores (2 nm $< d <$ 50 nm). CO_2 is thus more advantageous in producing an AC with a more uniform, predominantly microporous structure (Rashidi and Yusup, 2016). The use of CO_2 as an activated agent also offers a cheaper and more energy-friendly route than steam activation since this tends to require a steam generator whereas CO_2 activation does not (Rashidi and Yusup, 2016). To the best of our knowledge, this paper details for the first time the production and characterisation of CO_2-activated MCC-based sorbents for CO_2 capture, with a focus on ensuring that the AC possesses the necessary physical properties to provide substantial CO_2 capture. Producing an AC which meets these qualities from a globally widespread renewable feedstock would not only provide another valuable application for MCC, but also another promising sustainable sorbent material for carbon capture applications with the added benefit that the production procedure is more amenable to larger scales.

2. Materials and methods

2.1. Preparation

Powder MCC with particle size 51 μm were supplied by Merck as raw feedstock. Its conversion into activated carbon consists of two synthesis stages, carbonisation and activation. Samples were prepared in a quartz reactor sat within a Nabertherm tubular furnace (RT 50-250/11). The quartz reactor was connected to a flow controlled N_2 stream. During carbonisation (suffix 'C'), the raw microcrystalline cellulose was converted into a biochar by subjecting it to a heating ramp (10°C/min) from ambient temperature to 500°C under N_2 flow (80 Nml/min). The sample was then held at 500°C temperature for 1 hour before being cooled down under the same flowrate. A biochar was thus produced, denoted as sample μC5 to indicate its preparation at 500°C. Bio-oil (liquid product) formed during the carbonisation process was collected in a cold trap connected to the outlet of the reactor. Activation (suffix 'A') entailed the biochar being heated from ambient temperature at 10°C/min to 600°C under N_2 flow (80 Nml/min). Once this temperature had been reached the gas flow was switched to the activating agent, CO_2 (20 Nml/min), and activated to the target burn-off condition. of 10, 20 and 30%. Burn-off conditions were achieved from determining and using the appropriate residence time in activation conditions. ACs activated to burn-off conditions of 10% (1 hour), 20% (3 hours) and 30% (16 hours) were produced. Achieving a burn-off condition of 40% was found experimentally to exceed a duration of 24 hours, unlike the other burn off conditions (3-16 hours), hence a 40% burn-off condition and above were deemed as unviable from a process efficiency perspective.

Unlike in various other studies into ACs produced by physical activation that typically use activation temperatures of 800-1000°C to produce ACs with maximised performance (Abd et al., 2020), this study has avoided the use of such high activation temperatures, with the activation temperature kept 100°C above the carbonisation temperature. This in attempt to maintain a viable degree of feasibility of the process particularly for its future scaling up. Indeed, life cycle assessment studies in literature have emphasised that lower pyrolysis temperature increases the economic feasibility of a slow pyrolysis process (Azzi et al., 2019).

ACs produced are denoted as μC5A6 to indicate activation at 600°C and the sample code is completed with the addition of specific single digits to represent the burn-off condition for each AC. Thus, three AC samples μC5A6-1, μC5A6-2 and μC5A6-3 represent ACs samples of 10, 20 and 30 wt% burn-off conditions respectively. Each burn-off condition applied is to produce an AC that was developed with a unique activation route that can be assessed with regards to the nature of physical and textural property development of the resultant AC and its suitability for CO_2 capture and potential for incorporation into post-combustion carbon capture.

Commercial activated carbon Norit R2030CO2 (referred to as Norit R) was used for comparison with sorbents produced with regard to dynamic CO_2 adsorption performance (See subsection 3.8). Norit R is a peat-based commercial activated carbon (2-3mm particle diameter) supplied by Cabot Corporation, produced by steam activation and designed specifically for CO_2 capture.

2.2. Material characterisation

2.2.1. Thermal stability analysis

The thermal stability of the raw feedstocks, biochars and activated carbons were assessed using a Mettler Toledo 3+ Thermogravimetric Analyser (TGA). Approximately 20 mg of sample was placed in an aluminium oxide crucible which was inserted into the TGA furnace. Samples were subjected to a heating ramp (10°C/min) in a N_2 flow (50 Nml/min) from 25-1000°C and the mass (wt%) was recorded with increasing temperature, where decrements in the curve produced represented mass losses. Thermal stability data obtained provides insight

into material behaviour across preparation stages (i.e., carbonisation and activation) and activated carbon durability at temperatures above ambient/room temperature conditions.

2.2.2. Elemental analysis

Samples were subjected to an elemental analysis to determine C, H, N and O content. This was achieved using a Thermo Scientific FlashSmart analyser at the University of Birmingham. For their preparation before analysis, samples were oven-dried at 70°C for approximately two weeks.

2.2.3. FTIR spectroscopy

FTIR spectra were collected for each sample to characterise their structure. This procedure was completed using a Perkin-Elmer Spectrum Two FT-IR Spectrometer fitted with an attenuated total reflectance accessory. Spectra were generated in a wavenumber range of 450-4000 cm^{-1} with a scan resolution of 4 cm^{-1} and two scans per sample.

2.2.4. Point of zero charge

The point of zero charge (pH_{PZC}), the pH at which the surface charge is neutral (Bernal et al., 2018) is an indicator of surface acidity/basicity and was determined by a mass titration procedure adopted from Noh and Schwarz (Noh and Schwarz, 1989). Specifically, 0.250 g of sample were placed in a tube and suspended in distilled water, with increments of distilled water added daily. The remaining open space between the suspension and the tube was filled with N_2 to maintain an inert atmosphere within the tube, and the suspension stirred continuously at room temperature using a magnetic stirrer. Each day prior to adjusting mass concentration, the pH of the suspended samples was measured once equilibrium was reached. This procedure was carried out over a 10-day period before the pH_{PZC} was determined as an average of the most consistent range of pH values measured for each sample.

2.2.5. Surface morphology

The surface morphology and structure of biochars and activated carbons were observed by SEM imaging, using a Carl Zeiss GeminiSEM 300 analyser operated using a secondary electron imaging mode.

2.2.6. Adsorption isotherms

Adsorption isotherms have been used for the basis of characterisation of sample textural properties. N_2 isotherms were measured at -196°C with a Micrometrics TriStar 3000 analyser. From the data obtained, the total pore volume was calculated using Gurvich's law, the micropore volume and average pore dimensions were calculated using the Dubinin-Radushklevich (DR) equation and the specific surface area from the Brunauer Emmet Teller (BET) equation (Vargas et al., 2011). The mesopore volume was calculated as a difference between the micropore volume and the cumulative volume for a pore size 50 nm, obtained from pore size distribution data (Manyà et al., 2018). Pore size distributions based on N_2 isotherm data were determined using DFT model theory, with an assumption of slit-pore geometry. Additionally, CO_2 isotherms (measured at various temperatures) were collected using a Micrometrics ASAP 2020 analyser. CO_2 isotherms at 0°C were measured for the determination of the presence of ultra-micropores (< 0.7 nm) (Sethia and Sayari, 2015), which were estimated using the DR equation. Additional CO_2 isotherms were measured at 25, 30, 40 and 50°C to measure CO_2 adsorption capacities and to obtain the isosteric heat of adsorption, Q_{st} (kJ/mol) using the Clausius-Clapeyron equation depicted in Equation 2 (Manyà et al., 2018).

$$-\frac{Q_{st}}{R} = \left(\frac{\partial lnP}{\partial T}\right)_q \tag{2}$$

2.2.7. Dynamic CO_2 adsorption, and CO_2 / N_2 selectivity

Whilst CO_2 adsorption isotherms are beneficial for identifying the capture capacity potential of sorbents, these type of adsorption tests are performed discontinuously. Post-combustion streams of CO_2 will flow in continuous, dynamic flows hence it is important to observe how the capture potential identified from adsorption isotherms translates to adsorption under dynamic capture conditions. In addition to capture capacity, a suitable sorbent for post-combustion CO_2 capture will possess key characteristics such as high stability, ease of regeneration and suitable CO_2 selectivity (González et al., 2013). These characteristics are also assessable through dynamic CO_2 capture experiments. Therefore isothermal, CO_2 adsorption-desorption cycles were performed in the Mettler Toledo 3+ TGA. Each sorbent (~20mg) was loaded into a 100 μL aluminium crucible for insertion into the TGA furnace. The sample was first dried by heating at 10°C/min to 100°C under N_2 flow at 50ml/min before cooling to 25°C under the same N_2 flow. After mass stabilisation, at 25°C, the feed gas was switched from N_2 to CO_2 for isothermal capture until equilibrium was reached. With completion of the adsorption stage, the feed gas to the TGA was switched to N_2 and the sample heated to 100°C for regeneration before being cooled down to 25°C, allowing for the next adsorption cycle to occur. Mass vs time data was produced, from which the quantity of CO_2 adsorbed or desorbed was determined from the Equation 3 below:

$$Q_{CO_2} = \left(\frac{m_f - m_i}{m_i}\right) \div M_{CO_2} \tag{3}$$

where Q_{CO_2} is the total quantity of CO_2 adsorbed in mmol/g, m_i the initial mass of the sample, m_f the final mass of the sample, which is divided by M_{CO_2}, the molar mass of CO_2 (0.044095 g/mmol). In the case of adsorption, initial mass (m_i) is the mass recorded after pre-treatment/regeneration at 100°C and the final mass (m_f) as the mass at adsorption equilibrium. In the case of desorption, the initial mass is the mass equilibrium prior to its heating and then the final mass is the mass of the sample after regeneration when it has undergone desorption.

Other studies where sorbents have been tested in TGA-based CO_2 adsorption-desorption cycles have determined the sorbents tested to show promising stability with a total of 4-5 cycles of adsorption (Lahuri et al., 2022), (Choi et al., 2011), (Rao et al., 2018). In this study a total of 10 adsorption-desorption cycles were performed to evaluate sorbent subjected to dynamic capture conditions and the CO_2 adsorption/desorption performance of the MCC-sorbents was compared with that of Norit R, which was also subjected to this procedure.

The adsorption selectivity of CO_2 over N_2 was assessed. Cyclic N_2 adsorption-desorption tests were collected using an adsorption procedure equivalent to that described with CO_2. Any N_2 adsorbed during the regeneration cooling stage was deemed negligible. From this capture data, the selectivity of CO_2 over N_2 with varying temperature was obtained using Equation 4:

$$S = \frac{q_{CO_2}}{q_{N_2}}\,\sigma \tag{4}$$

where S is the apparent selectivity, q is the quantity (mmol/g) adsorbed at 101.3 kPa over the adsorption step after 1 minute, which is within the usual residence time of a swing adsorption process, and σ is the ratio of CO_2 adsorbed at 15 kPa to at 101.3 kPa from the corresponding adsorption isotherm (Manyà et al., 2018). This calculation of selectivity is not to be compared with selectivity calculated from adsorption isotherms or with Ideal Adsorbed Solution Theory (IAST) for binary mixtures, but instead offers an initial estimation of CO_2 selectivity over N_2 (Manyà et al., 2018). González et al. (Chao et al., 2021) reported that the uptake of the weaker adsorbate (N_2 in this case) is lower in multicomponent adsorption systems (González et al., 2013), (Garba et al., 2020) such as post-combustion streams, hence this calculation will provide an initial indication of a selectivity, which can only be bettered upon furthering the experimental assessment of sorbents into post-combustion conditions.

3. Results and discussion

For the carbonisation of microcrystalline cellulose, biochars were produced with an average biochar yield of 25 wt%, an average bio-oil yield of 40 wt% and a 35 wt% yield of gaseous product. The later was calculated from the difference of the original raw MCC weight and the sum of the biochar and bio-oil masses. ACs of three burn-off conditions were produced. As expected, the cellulose samples transform from their white fine powder from, into a black, carbonaceous, fine powder form ($\leq$ 51 μm) upon carbonisation and activation.

3.1. Thermal stability analysis

Fig. 1 depicts the mass (wt%) against temperature curves of raw MCC in addition to the biochar and activated carbon samples produced. For the degradation profile of raw MCC, an initial decrease was observed in the temperature range of 60-140°C, which indicates the loss of moisture (Trache et al., 2014). A substantial decrease in mass was observed in the temperature range 300-450°C where the glycosyl units of the MCC are broken down through various decomposition reactions including dehydration, decarboxylation, decarbonylation and depolymerisation as char product is formed (Trache et al., 2014), (Xin et al., 2015). During carbonisation experiments, bio-oil formation was observed in the temperature range 300-400°C, in agreement with observations reported elsewhere for the pyrolysis of cellulose (Zhang et al., 2021). At temperatures above 450°C the sample mass becomes fairly stable, likely due to char formation. The thermal profiles of the sorbents produced are all very similar regarding shape and thus degradation behaviour. The profile of the biochar μC5 that was obtained by carbonisation of raw MCC at 500°C, shows a more stable thermal profile in comparison to raw MCC. Unlike raw MCC, which loses 90.4 wt% of its mass through thermal degradation in a range of 25-1000°C, the biochar μC5 that was obtained by carbonisation at 500°C loses only 16.1 wt% of its mass in this same temperature range. Notably, degradation begins at temperatures above 500°C, with the predominant reactions likely being deoxygenation and dehydrogenation as the content of aromatic ring groups within the biochar increases (Xin et al., 2015). The AC samples which were prepared at higher temperatures (and during longer activation times, i.e. increasing burn-off), showed even greater thermal stability, with degradation starting at progressively higher temperatures with increasing burn-offs. Based on the thermal profiles produced, whilst the carbonisation temperature used in production certainly guarantees sufficient biochar development, the moderate activation temperature used should also be suitable enough to contribute to sufficient materials conversion for porous sorbent development.

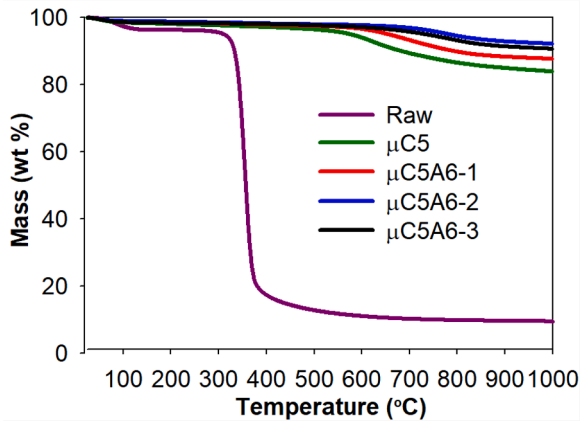

Fig. 1. TGA profiles of raw MCC and MCC-based sorbents.

3.2. Elemental analysis and point of zero charge

The evolution of MCC from its raw form into a sorbent is reflected by elemental analysis data shown in Table 1. The composition of raw MCC matches closely to that which is expected for cellulose ($(C_6H_{10}O_5)_n$), whilst the composition of char shows the carbon content more than doubles relative to MCC. The sizeable reduction in oxygen content together with a smaller reduction in hydrogen content is consistent with the decomposition reactions previously described. With increasing burn-off, a slight increase in carbon content is observed, with the highest carbon content of 91.23 wt% being exhibited by AC μC5A6-3. Reduction in hydrogen content is also evidence of the occurrence of aromatisation in the formation of these MCC-based sorbents (Zhang et al., 2021).

The point of Zero-charge, pH_{PZC}, for each sorbent was measured and results are presented in Table 1, displaying the surface character of the sorbents to be close to neutrality.

3.3. FTIR spectroscopy

The FTIR spectra for the samples are shown in Fig. 2. Raw MCC shows a band at 3333 cm^{-1}, corresponding to OH stretching vibrations indicative of alcohol and phenol groups (Colthup, 1990), (Kassanov et al., 2017). A smaller band at 2893 cm^{-1} represents aliphatic C-H stretching vibrations, particularly that of a methyl group in the glucopyranose ring of a cellulosic structure (Colthup, 1990), (Xin et al., 2015). A band is observed at 1653 cm^{-1} and is assigned to C=O double bond stretching vibrations, indicative of the presence of carbonyl groups. The band at 1428 cm^{-1} suggests the presence of methyl and methylene groups next to a carbonyl group (Colthup, 1990). The band at 1320 cm^{-1} corresponds to CH_2 wagging vibrations and is again typical of methylene groups found in hydrocarbon chains (Colthup, 1990). The larger band at 1031 cm^{-1} is indicative of C-O-C stretching vibration associated with the pyranose ring structure of cellulose (Kian et al., 2017).

The IR spectra profiles of the sorbents exhibit bands with weaker intensities and at mostly different wavenumbers compared to raw MCC, reflecting expected changes to the functional group composition during carbonisation and activation. The IR spectra profiles of all the sorbents show close similarity, indicating that carbonisation process is predominantly responsible for introducing major changes to the raw MCC as it is converted into sorbent form. Bands at 1580 cm^{-1} indicate C=C stretching vibrations, assigned to the presence of aromatic structures within the sorbents (Xin et al., 2015). The peaks at 1031 cm^{-1} correspond once again to C-O stretching band but occur with lesser intensity than for fresh MCC. This is again consistent with the expected transformation during carbonisation. Aromatic C-H wagging mode is apparent in the wavenumber range of 740-900 cm^{-1}, once again indicating the occurrence of aromatisation (Colthup, 1990). The band at 1054 cm^{-1} present for AC μC5A6-3 is indicative of the C-O stretch vibration of a hydroxyl group (Xin et al., 2015), whilst aliphatic methyl structures are also identifiable from the C-H stretch vibration identifiable by the band at 2877 cm^{-1} (Colthup, 1990). The formation of aromatic structures within this AC is further evident from the C-H stretching vibration represented by the band at 2983 cm^{-1} (Xin et al., 2015).

Table 1
Sample elemental composition (wt%) & Point of Zero charge.

Sample	C	H	N	O	$pH_{,PZC}$
Raw MCC	42.20	6.35	0.00	51.46	-
μC5	85.03	3.04	0.00	11.94	7.22
μC5A6-1	88.95	2.62	0.00	8.44	7.18
μC5A6-2	88.96	1.56	0.00	9.48	7.16
μC5A6-3	91.23	1.76	0.00	7.01	6.95

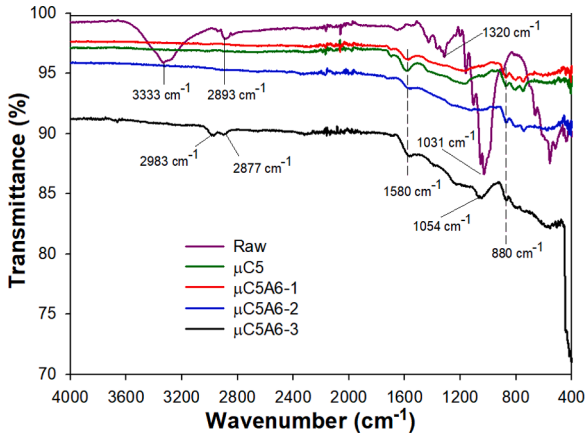

Fig. 2. FTIR spectra of raw MCC and MCC-based sorbents.

3.4. Surface morphology

Figs. 3a-c displays the SEM images of raw MCC, μC5 and μC5A6-3. The lower image magnification (x100) of raw MCC depicts its fibrous structure, with higher magnification (x500) revealing its amorphous, rough surface structure. This structure is maintained through carbonisation and activation as shown in Figs. 3b and c, indicative of the substantial structural stability associated with MCC. More detailed physical changes however can be identified through analysing their textural properties from the adsorption isotherms.

3.5. Adsorption isotherms and textural properties

3.5.1. N_2 adsorption isotherms

Fig. 4 depicts the N_2 isotherms measured at -196°C and a complete summary of the textural properties is presented in Table 2. The isotherm shapes show a Type I IUPAC shape with the isotherm not plateauing until a relative pressure of around 0.1, which indicates the presence of large micropores and/or small mesopores (Serafin et al., 2017). This is reflected in the calculated textural properties presented in Table 2. The biochar μC5 shows the lowest N_2 adsorption capacity and pore volume, indicating that the ACs still undergo substantial pore development during activation, with AC μC5A6-3 presenting the highest N_2 adsorption capacity. Textural property calculations confirm the presence of micropores, as suggested by the shape of the N_2 isotherm of the sorbents. The micro/total pore volumetric ratio remains constant regardless off burn-off condition, however with increasing burn-off the pore distribution tends to become narrower, whilst properties such as specific surface area, micro and total pore volume increase. Notably, a relative increase of 50% in the ultramicropore volume is observed when comparing the μC5 and μC5A6-3. This clearly shows that there is a tendency to create smaller micropores with the increase in the burn-off, which is expected to favour CO_2 adsorption. Pore Size Distribution (PSD) data for N_2 isotherms in Fig. 5 confirm that sorbents consist predominantly of a combination of micropores and smaller mesopores. The textural properties investigated for the MCC-based sorbents are recorded in Table 4, along with that of other ACs obtained from literature. Compared to the ACs recorded in literature, the MCC-based sorbents produced possess lower, more moderate specific surface areas (400-500 m^2/g) compared to the ACs in literature (360-2430 m^2/g). The small variation in the textural properties observed amongst the MCC-based sorbents produced, particularly specific surface area and the total pore volumes, is attributable to the moderate 600°C activation temperature. Despite the moderate activation temperature, these ACs along with biochar μC5 do possess substantial microporosity, which is of more importance in the context of CO_2 adsorption under post combustion conditions (Manyà et al., 2018). Furthermore, the notable increase in ultramicropore volume with an increase in activation burn-off suggest an improvement of the produced sorbents for their application in post-combustion capture processes (Martín et al., 2010), (Martín et al., 2011). This is of course, evidenced by the CO_2 adsorption data produced (see next).

3.5.2. CO_2 adsorption isotherms

CO_2 isotherm data collected at temperatures in the range 0-50°C are depicted in Fig. 6a-d. The maximum adsorption capacities are recorded in Table 3 with characteristic energies mentioned, whilst ultramicropore textural properties calculated from isotherm data at 0°C are included in Table 2. It is evident that ultramicropore volume increases with activation burn-off and the pores tend to narrow in size (although this is a lesser effect than the increase in pore volume), confirming pore development trends conveyed from N_2 adsorption isotherm data. Regarding CO_2 adsorption capacities, μC5A6-3 possesses the highest CO_2 adsorption capacity at all temperatures, which can be attributed to both its narrowest ultramicropore structure and highest ultramicropore volume amongst all the sorbents. The decrease in CO_2 adsorption capacity with increased temperature highlights that the adsorption process is exothermic in nature (Guo et al., 2020). The narrowing in pore width corresponds to increases in the characteristic energy with increasing burn-off as shown in Table 3, which together with the CO_2 adsorption capacities recorded confirm an increase in adsorption affinity with increasing burn-off.

The CO_2 adsorption capacities have been included alongside the key textural properties of these MCC-based sorbents in Table 4. The CO_2 adsorption capacities from sorbents in literature have been included. These CO_2 adsorption capacities are also represented visually in Fig. 8. Perhaps expectedly, the largest CO_2 adsorption capacities are from ACs produced by chemical activation (water chestnut shell). Whilst valuable for providing a fairer comparison and assessment of the capturing capability of the sorbents produced in this study, as highlighted previously, ACs produced by chemical activation are a less environmentally favourable option at larger scale compared to physically activated ACs. Whilst not the best performing in terms of CO_2 adsorption capacity compared to the other ACs listed, including those produced by physical activation, the adsorption capacities of these MCC-based sorbents are within a comparable range. This is evident particularly in comparison to ACs produced from cladophora cellulose, olive mill waste, palm kernel shell and sugar cane bagasse, as well as commercial ACs Norit®SX2 and commercial granular AC, which are all sorbents that have been identified as promising for CO_2 capture. Where MCC-based ACs are more advantageous, particularly compared to the ACs from lignocellulosic feedstocks such as sugar cane bagasse, vine shoots and water chestnut shell, is that their abundance and greater global prevalence offers a more accessible and feasible option, particularly for production of sorbents in larger quantities that meet pilot or commercial scale.

It is noticeable that commercial granular AC, despite possessing a substantially larger specific surface area and pore volumes compared to the MCC-based sorbents, has a lower CO_2 adsorption capacity. This can be attributed to its smaller micropore presence and larger average pore width compared to the MM-based ACs, thus highlighting the importance of a narrow pore size presence within sorbents (Martín et al., 2010), (Martín et al., 2011).

3.6. Isosteric heats of adsorption

Fig. 7 depicts the isosteric heat of adsorption (Q_{st}) calculated for CO_2 with each sorbent. Firstly, all Q_{st} values presented by the sorbents are all well below 80 kJ/mol, which confirms that physisorption is the adsorption mechanism occurring (Chowdhury et al., 2011). Variations in Q_{st} with surface loading indicate a heterogeneous surface energy is present (Manyà et al., 2018). In the case of carbonaceous sorbents, this can be attributed to its pore size distribution, which leads to the presence of adsorption sites with different adsorption enthalpies (Manyà

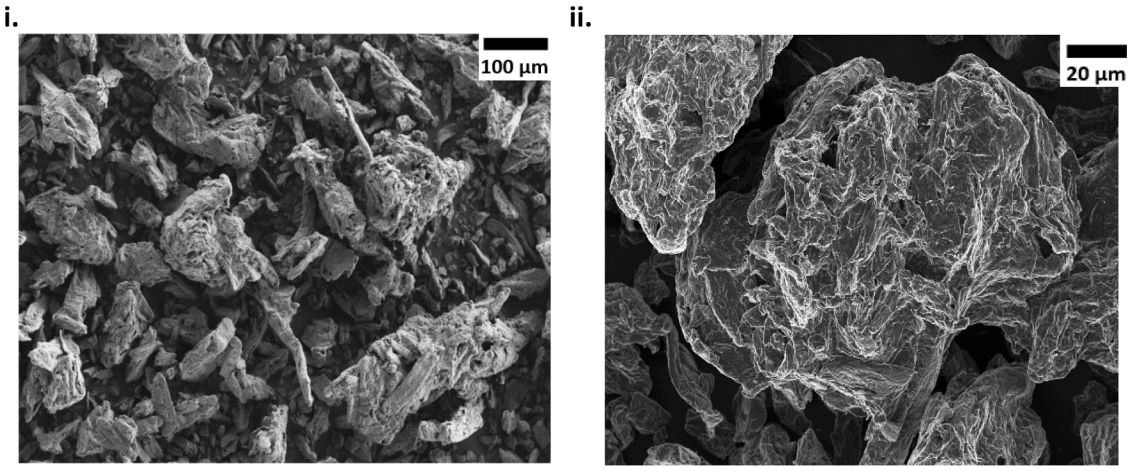

a: SEM images for µ at magnifications i. x100 ii. ×500

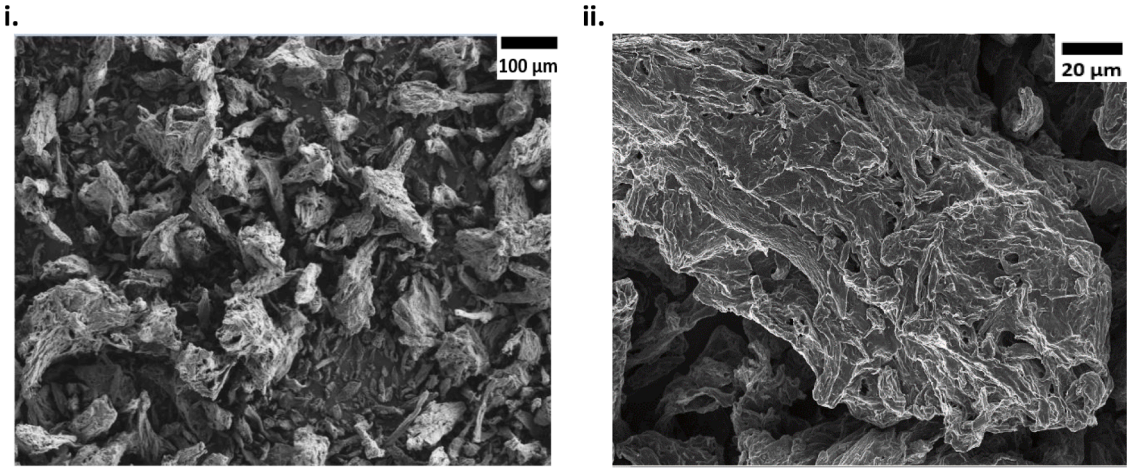

b: SEM Imaging for µC5 at magnifications i. x100 ii. ×500

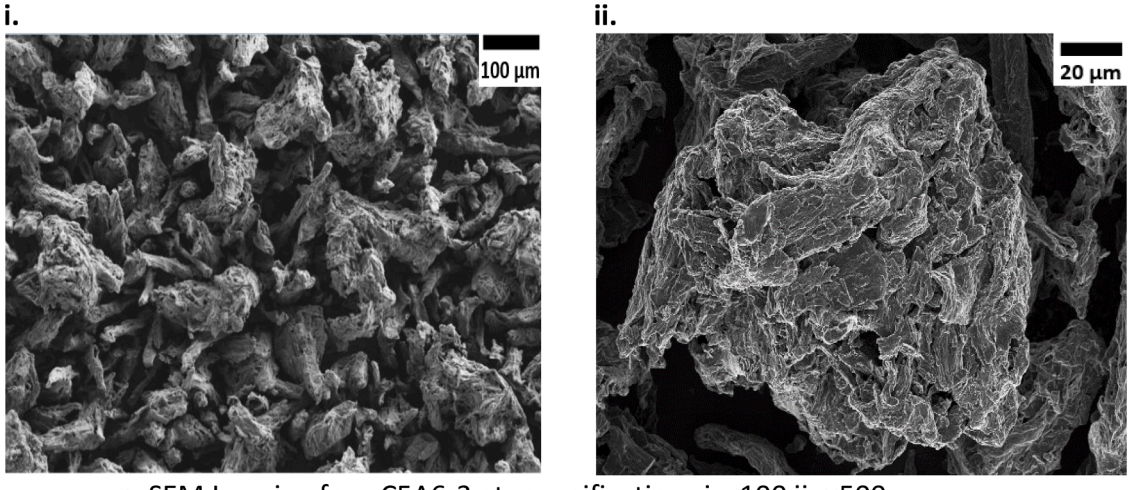

c: SEM Imaging for µC5A6-3 at magnifications i. x100 ii. ×500

Fig. 3. a. SEM images for µ at magnifications i. x100 ii. × 500. b. SEM Imaging for µC5 at magnifications i. x100 ii. × 500. c. SEM Imaging for µC5A6-3 at magnifications i. x100 ii. × 500.

et al., 2018), (González et al., 2013). In the case of all MCC-based sorbents produced in this research, they show a non-uniform distribution of pore sizes with micro, meso and macropores found in each sorbent, hence the heterogeneous surface adsorption behaviour displayed (Bernal et al., 2018). Typically, observed with many sorbents recorded in literature that display heterogenous adsorption behaviour is a decrease in Q_{st} with increased CO_2 loading. This is usually due to higher Q_{st} indicating filling of narrower pore structures such as ultramicropores whilst lower Q_{st} reflects interactions in larger pore structures (Manyà et al., 2018). In the case of these sorbents, the increase of Q_{st} with increased CO_2 loading is indicative of reinforced adsorbate-adsorbent intermolecular interactions and possible multilayer adsorption of CO_2 (Plaza et al., 2014), (Guo et al., 2018). AC µC5A6-3 showed the highest Q_{st}, at least at lower CO_2 loadings, due to its narrower pore structure

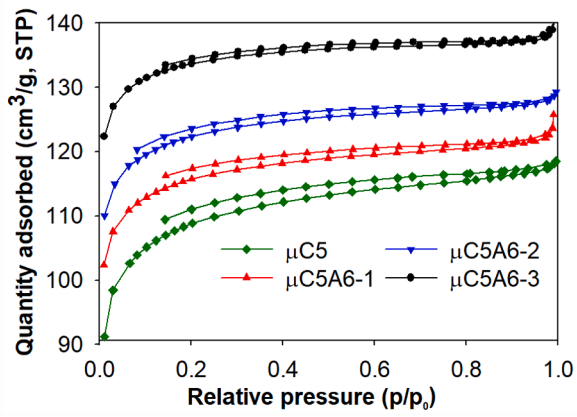

Fig. 4. N_2 adsorption isotherms at -196°C for μ-derived sorbents.

compared to the other sorbents (González et al., 2013). Table 4 summarises the Q_{st} values of other physical activated carbons and commercial sorbents investigated for CO_2 capture. The MCC sorbents prepared in this work generally show higher heat of adsorption values (38-55 kJ/mol) when compared to the other sorbents in Table 5 (25-42 kJ/mol), with quantities only in a similar range for sugar-cane bagasse derived AC (41.9 kJ/mol). This is indicative of strong affinity and hence bonding between CO_2 molecules and adsorption sites, attributable to the substantial micropore presence in MCC sorbents compared to all the other sorbents presented in Table 4, and the presence of ultramicropores as previously highlighted. Whilst the high affinity is a strength of the MCC-ACs with regards to CO_2 capturing capability, this also may provide a potential limitation to the energy feasibility associated with these sorbents, particularly in the energy requirement needed for the thermal regeneration of the sorbent in a cyclic adsorption process. However, these values are still lower than Q_{st} values for amines, which operate with chemisorption mechanisms and are found to record Q_{st} values close to 100 kJ/mol (Plaza et al., 2014). Hence whilst the Q_{st} values for these MCC-based ACs appear relatively high for solid sorbents based on the Q_{st} of the other sorbents recorded in Table 4, they are still substantially lower when compared to commercially utilised amine-based solvent and as mentioned previously, can produce considerably substantial CO_2 capture capacities. From this finding it is clearly worth further investigating the capture potential of the MCC-based sorbents produced by testing adsorption under dynamic conditions.

3.7. Dynamic adsorption-desorption cycles

The adsorption CO_2 adsorption/desorption cycles are depicted in Fig. 9, expressed over the full 10 cycle adsorption-desorption period. Adsorption at 25°C is clearly observed where the curve rises and then reaches equilibrium as shown by the flat peaks of the curves. The sharp decrease in the curve after reaching equilibrium represents the stage at which desorption at 100°C occurs. Table 5 summarises the 10-cycle aggregated adsorption and desorption quantities for each sorbent, and an average CO_2 adsorption/desorption capacity per cycle, justifiable based on the close consistency of CO_2 adsorbed and desorbed over each cycle. All MCC-based sorbents, show stable capture capacity over 10 cycles as previously highlighted, with minor fluctuations (±2%) only noticeable for μC5A6-1 and μC5. Total and average CO_2 adsorption capacities obtained show CO_2 adsorption capacity to increase upon activating the biochar and with increasing activation burn-off condition, a trend previously observed in static adsorption tests. Increases in CO_2

Table 2
MCC sorbent textural properties obtained from adsorption isotherms generated from N_2 at -196°C (a-g) and CO_2 at 0°C (h-i)

Sample	S_{BET} [a] (m^2/g)	W_T [b] (cm^3/g)	W_0 [c] (cm^3/g)	W_0/W_T [d]	W_{meso} [e] (cm^3/g)	D [f] (nm)	L_0 [g] (nm)	$W_{0,\ ultra}$ [h] (cm^3/g)	$L_{0,ultra}$ [i] (nm)
μC5	403	0.18	0.17	0.95	0.02	1.82	1.46	0.18	0.62
μC5A6-1	434	0.19	0.18	0.95	0.02	1.78	0.94	0.21	0.61
μC5A6-2	443	0.20	0.19	0.95	0.03	1.80	0.72	0.23	0.61
μC5A6-3	487	0.21	0.20	0.95	0.03	1.72	0.63	0.27	0.59

[a] Specific surface area
[b] Total pore volume
[c] Total micropore volume
[d] Micropore volume ratio
[e] Total mesopore volume
[f] Average pore diameter
[g] Average micropore width
[h] Ultramicropore volume
[i] Average ultramicropore width

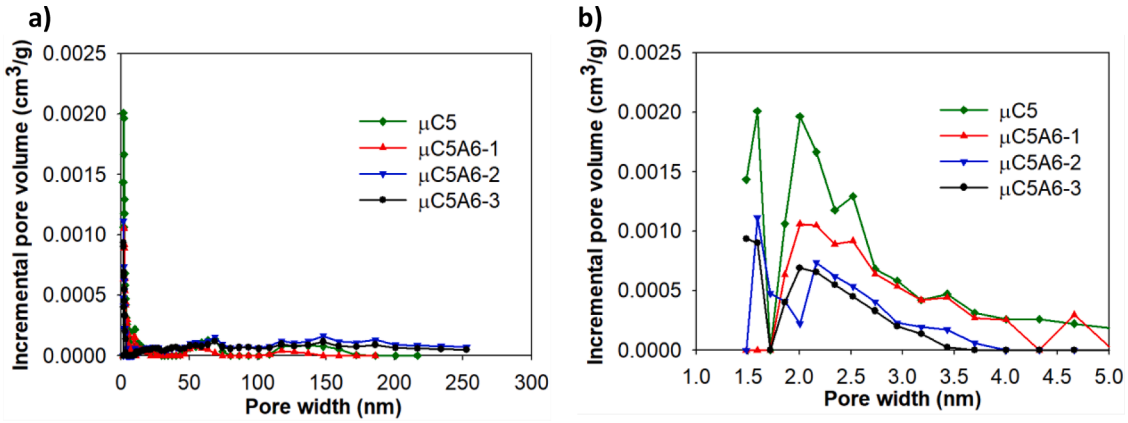

Fig. 5. Pore size distribution (incremental) for MCC sorbents depicted across **a)** Full range **b)** narrower pore range.

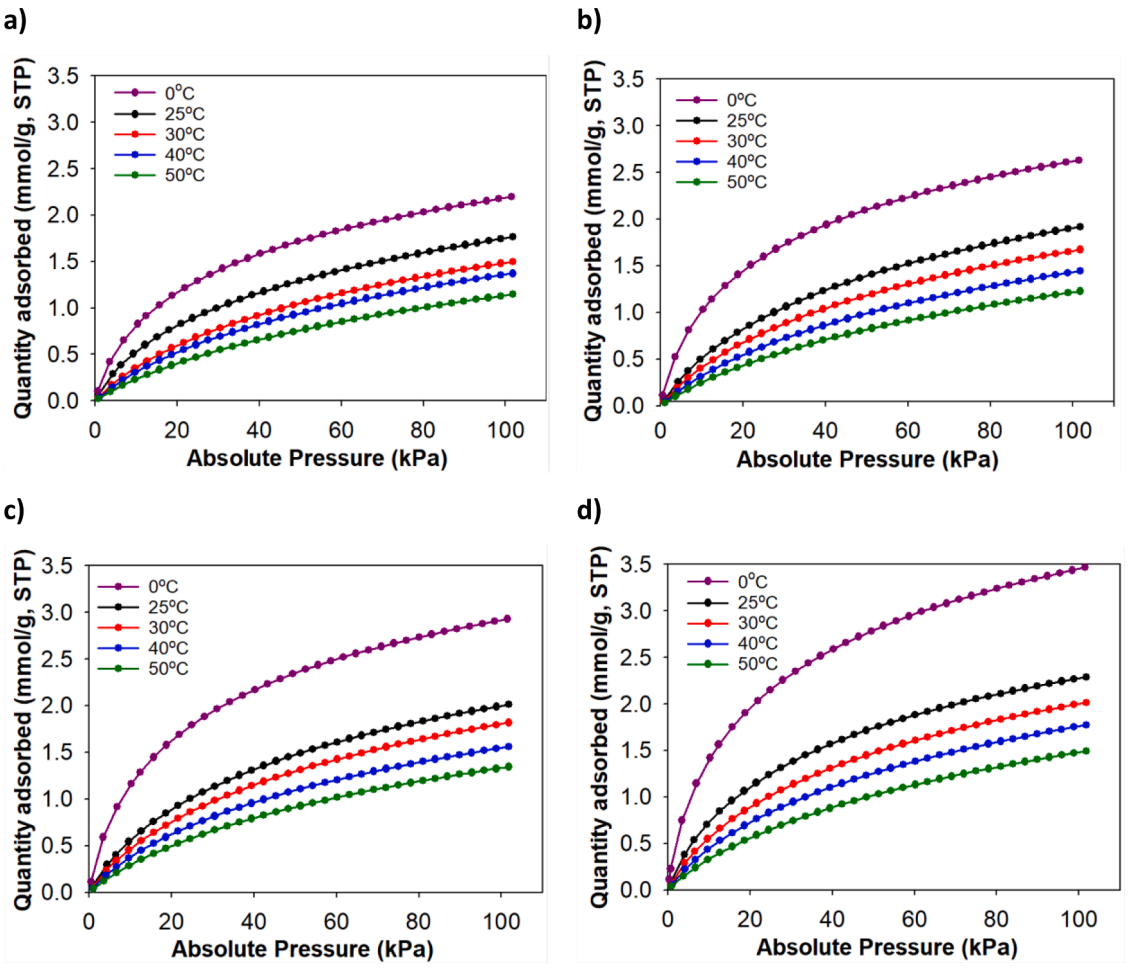

Fig. 6. CO_2 adsorption isotherms for μC5 (a), μC5A6-1 (b), μC5A6-2 (c), and μC5A6-3 (d).

Table 3
MCC sorbent CO_2 adsorption capacities 0-50°C and characteristic energy, E_0.

Sample	0°C (mmol/g)	25°C (mmol/g)	30°C (mmol/g)	40°C (mmol/g)	50°C (mmol/g)	E_0 (kJ/mol)
μC5	2.20	1.77	1.50	1.38	1.15	28.77
μC5A6-1	2.63	1.82	1.67	1.44	1.23	29.10
μC5A6-2	2.93	2.01	1.82	1.56	1.34	29.23
μC5A6-3	3.47	2.18	1.87	1.76	1.49	29.74

adsorption-desorption capacity is most pronounced between μC5 and μC5A6-1, (~30% increase) compared to the differences between other consecutive burn-off stages (~16% average). Not only does this indicate the effectiveness of the activation procedure in enhancing the sorbent CO_2 adsorption capability, but also further highlights the importance of narrowing the sorbent pore size (of micropore classification) to maximise CO_2 capture at post-combustion conditions, which this activation procedure clearly promotes. Average and total desorption capacities obtained for these sorbents indicate their possessing of substantial desorption capacity (> 98% of the CO_2 adsorbed).

The cyclic stability of these MCC-based sorbents is promising not only compared to Norit R, but also the CO_2 adsorption-desorption behaviour of other sorbents in literature. For instance, Lahuri et al. subjected Bismuth (III) oxide-impregnated ACs to CO_2 adsorption in a TGA at ambient conditions, obtaining similar cyclic stability over 5 cycles, however this was achieved with a regeneration temperature of 900°C (Lahuri et al., 2022). These MCC-based ACs also show promising stability compared to the CO_2 adsorption-desorption behaviour of silica supported polyethyleneimine (silica PEI) sorbents studied by Choi et al. In adsorbing CO_2 similar adsorption conditions in a TGA, sorbents encountered fluctuations in their CO_2 adsorption capacity in the range of 2-8%, over 4 adsorption-desorption cycles, with a more similar regeneration temperature (110°C) applied (Choi et al., 2011).

Whilst showing substantial stability across its adsorption-desorption cycles, these MCC-based ACs do possess lower CO_2 adsorption capacities under dynamic conditions than when measured with adsorption isotherms, which were static (maximum capacity at equilibrium). This can be accounted for by CO_2 molecules gaining more mobility under increased flow rates (dynamic conditions), causing more forced molecular movements and less retention of CO_2 on the sorbent (Ramos et al., 2022), (Abdullah and Qasim, 2016). In addition, the TGA is not necessarily designed specifically for CO_2 capture, hence scaled-up systems more specifically designed for capture, such as a fixed or fluidised bed, may yield a slightly different performance of the sorbents under dynamic conditions. Regarding the MCC-based sorbents, they all appear to show stable capture capacity over 10 cycles as previously highlighted, with minor fluctuations (±2%) only noticeable for μC5A6-1 and μC5. Also recorded is the adsorption and desorption data for commercial sorbent Norit R, which μC5A6-3 exhibits similar adsorption/desorption performance and stability. This is highlighted further in Table 5 which compares the adsorption/desorption performance per cycle of the two sorbents. Overall, both sorbents show very similar adsorption-desorption capability, with slight variations (~1%) in the

Table 4
Comparison of CO_2 capacity at 25°C and Q_{st} of MCC-sorbents with physically activated carbon and commercial sorbents reported in literature.

Sample	Activating agent	Key textural properties	CO_2 adsorption capacity (mmol/g) at 0°C and 25°C	Q_{st} (kJ/mol)	Ref.
μC5	-	S_{BET}= 403 m^2/g W_T = 0.18 cm^3/g W_0 = 0.17 cm^3/g W_{ultra} = 0.18 cm^3/g L_0 = 1.46 cm^3/g $L_{0,ultra}$ = 0.62 nm D = 1.82 nm	2.20 (0°C) 1.77 (25°C)	38.4	This work
μC5A6-1	CO_2	S_{BET} = 434 m^2/g W_T = 0.19 cm^3/g W_0 = 0.18 cm^3/g W_{ultra} = 0.21 cm^3/g L_0 = 0.94 nm $L_{0,ultra}$ = 0.61 nm D = 1.78 nm	2.63 (0°C) 1.82 (25°C)	38.0	This work
μC5A6-2	CO_2	S_{BET} = 443 m^2/g W_T = 0.20 cm^3/g W_0 = 0.19 cm^3/g W_{ultra} = 0.23 cm^3/g L_0 = 0.72 cm^3/g $L_{0,ultra}$ = 0.61 nm D = 1.80 nm	2.93 (0°C) 2.01 (25°C)	44.9	This work
μC5A6-3	CO_2	S_{BET}= 487 m^2/g W_T = 0.21 cm^3/g W_0 = 0.20 cm^3/g W_{ultra} = 0.27 cm^3/g L_0 = 0.63 nm $L_{0,ultra}$ = 0.59 nm D = 1.72 nm	3.47 (0°C) 2.18 (25°C)	54.5	This work
Cladophora cellulose	N_2	S_{BET}= 500 m^2/g W_T = 0.62 cm^3/g W_0 = 0.15 cm^3/g W_{ultra} = - L_0 = - $L_{0,ultra}$ = - D = -	2.64 (0°C)	31.5	(Xu et al., 2018)
Dialdehyde cellulose	CO_2	S_{BET}= 1241 m^2/g W_T = 0.53 cm^3/g W_0 = 0.43 cm^3/g W_{ultra} = 0.29 cm^3/g L_0 = - $L_{0,ultra}$ = - D = -	5.52 (0°C)	32.1	(Xu et al., 2018)
Chitosan cross-linked cellulose	CO_2	S_{BET}= 832 m^2/g W_T = 0.36 cm^3/g W_0 = 0.29 cm^3/g W_{ultra} = 0.24 cm^3/g L_0 = - $L_{0,ultra}$ = D = -	4.97 (0°C)	28.5	(Xu et al., 2018)
Commercial granular AC	-	S_{BET} = 1727 m^2/g W_T = 1.204 cm^3/g W_0 = 0.578 cm^3/g W_{ultra} = - L_0 = 1.3 nm $L_{0,ultra}$ = - D =-	1.89 (25°C)	-	(Bezerra et al., 2011)
Norit®SX2	Steam	S_{BET}= 660.7 m^2/g W_T = 0.67 cm^3/g W_0 = - W_{ultra} = - L_0 = - $L_{0,ultra}$ = - D = 4.42 nm	1.88 (25°C)	27-28	(Rashidi and Yusup, 2017)
Palm Kernel Shell AC	CO_2	S_{BET} = 367.8 m^2/g W_T = 0.22 cm^3/g W_0 = - W_{ultra} = - L_0 = - $L_{0,ultra}$ = - D = 2.39 nm	2.13 (25°C)	27-28	(Rashidi and Yusup, 2017)
Sugar cane bagasse AC	CO_2	S_{BET}= 622 m^2/g W_T = 0.38 cm^3/g W_0 = 0.30 cm^3/g W_{ultra} = - L_0 = -	5.50 (0°C) 2.55 (25°C)	41.9	(Guo et al., 2020)

(continued on next page)

Table 4 (*continued*)

Sample	Activating agent	Key textural properties	CO_2 adsorption capacity (mmol/g) at 0°C and 25°C	Q_{st} (kJ/mol)	Ref.
		$L_{0,ultra}$ = D = 2.42 nm			
Vine shoots AC	CO_2	S_{BET} = 767 m^2/g W_T = 0.37 cm^3/g W_0 = 0.25 cm^3/g W_{ultra} = 0.11 cm^3/g L_0 = - $L_{0,ultra}$ = - D = -	4.07 (0°C) 3.0 (25°C)	25.5 27.5	(Manyà et al., 2018)
Rice husk AC	CO_2	S_{BET}= 1097 m^2/g W_T = 0.83 cm^3/g W_0 = 0.34 cm^3/g W_{ultra} = - L_0 = - $L_{0,ultra}$ = - D = -	3.10 (25°C)	-	(Li and Xiao, 2019)
Olive mill waste AC	CO_2	S_{BET}= 1135 m^2/g W_T = 0.48 cm^3/g W_0 = 0.37 cm^3/g W_{ultra} = 0.15 cm^3/g L_0 = - $L_{0,ultra}$ = - D = -	2.94 (0°C)	-	(González and Manyà, 2020)
Pine saw dust	KOH	S_{BET}= 2330.9 m^2/g W_T = 1.91 cm^3/g W_0 = 0.98cm^3/g W_{ultra} = - L_0 = - $L_{0,ultra}$ = - D =3.28	4.21 (25°C)	-	(Quan et al., 2020)
Raw bamboo	H_3PO_4	S_{BET}= 1503.2 m^2/g W_T = 0.64 cm^3/g W_0 = 0.57cm^3/g W_{ultra} = 0.15 cm^3/g L_0 = - $L_{0,ultra}$ = - D = 2.45 nm	1.45 (25°C)	-	(Rashidi and Yusup, 2017)
Tea seed shell	KOH	S_{BET}= 1503.2 m^2/g W_T = 0.64 cm^3/g	3.15 (25°C)	-	(Quan et al., 2020)

Table 4 (*continued*)

Sample	Activating agent	Key textural properties	CO_2 adsorption capacity (mmol/g) at 0°C and 25°C	Q_{st} (kJ/mol)	Ref.
		W_0 = 0.57cm^3/g W_{ultra} = - L_0 = 0.52 $L_{0,ultra}$ = - D = 2.45 nm			
Water chestnut shell	KOH	S_{BET}= 1353 m^2/g W_T = 0.38 cm^3/g W_0 = - W_{ultra} = - L_0 = - $L_{0,ultra}$ = - D = -	6.31 (0°C) 4.54 (25°C)		(Ma et al., 2022)

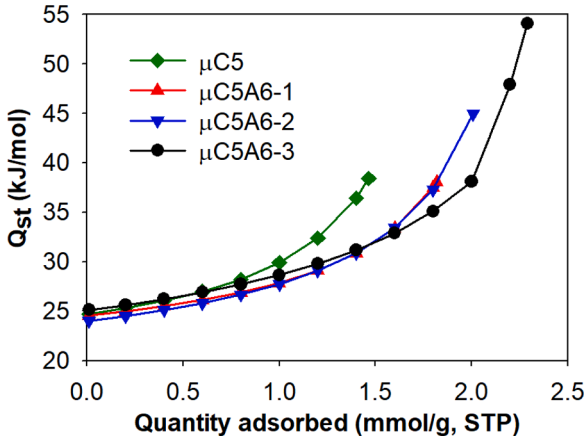

Fig. 7. Isosteric heat of adsorption of CO_2 for MCC samples.

total amount of CO_2 desorbed between the two sorbents. As the sorbents show substantial cyclic stability over 10 cycles, tests with a substantially larger number of cycles numbers will need to be completed prior to scale up to understand the long-term cyclic potential of the sorbent.

Regarding the use of Norit R, to reiterate, this sorbent is designed specifically for CO_2 capture, and its CO_2 capture has been explored extensively in literature at larger laboratory scales than those used in this study (Yassin et al., 2021), (Plaza et al., 2010), (Yassin et al., 2021). Norit R thus serves as an appropriate 'Benchmark AC' to justify further development of these sorbents. Also of key consideration upon scale-up will be the desorption procedure applied. In this TGA adsorption-desorption procedure, the N_2 used during regeneration as 'sweeping gas', whilst beneficial in identifying the desorption potential of these sorbents, would likely produce a largely diluted CO_2 desorption stream. Whilst dilute streams from carbon capture have been identified as suitable for use in greenhouse fertilisation or algae farming, most post-combustion capture routes will require desorbed CO_2 streams that are highly concentrated for transport and storage (Zerobin and Prö, 2020). As highlighted, this challenge has been sought to be addressed in research through adjusting the desorption conditions. Such a consideration adds to the importance of comparing the adsorption capability of these sorbents with Norit R, which has been experimented with in larger, more practical experimental scales where such solutions have been

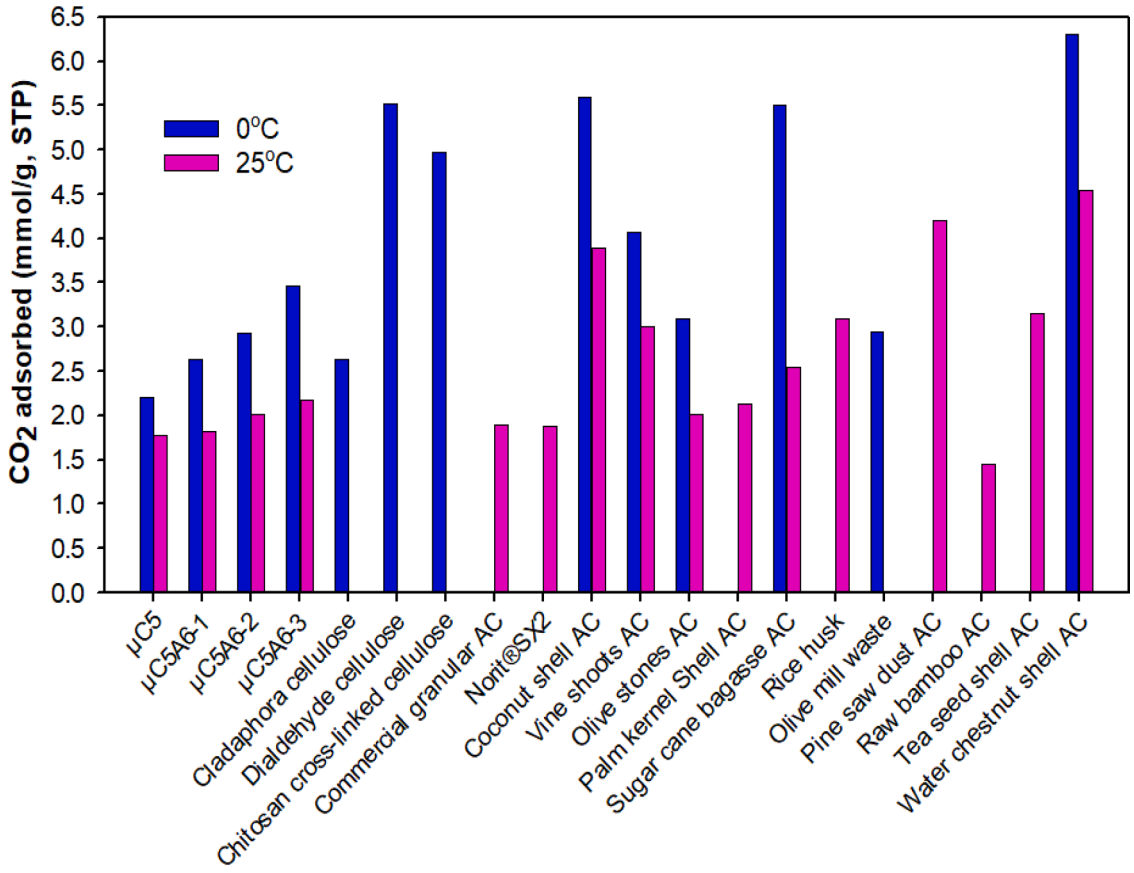

Fig. 8. CO_2 adsorption capacity comparison of MCC-sorbents with physically activated carbon and commercial sorbents reported in literature.

Table 5
Sorbent 10-cycle CO_2 adsorption and capacities.

Sample	Total CO_2 adsorbed	Average single cycle quantity of CO_2 adsorbed	Total CO_2 desorbed	Average single quantity of CO_2 desorbed
μC5	9.0	0.90	9.0	0.90
μC5A6-1	11.7	1.17	11.7	1.17
μC5A6-2	13.7	1.37	13.5	1.35
μC5A6-3	15.8	1.58	15.5	1.55
Norit R	15.8	1.58	15.7	1.57

explored. This includes experiments by Yassin et al. who in successfully conducting temperature swing adsorption tests with Norit R, used a substantially reduced sweeping gas flow rate (20% of the adsorption flow rate) during desorption (Yassin et al., 2021). Considering the similarity in performance of MCC-derived sorbents such as μC5A6-3 to Norit R, this would be a route likely to be considered in the scaling up CO_2 adsorption-desorption tests, as part of improving the feasibility, and practicality of the use of these new sorbents in the separation process.

3.8. CO_2 / N_2 apparent selectivity

Table 6 depicts the apparent selectivity of the sorbents along with the CO_2 adsorbed after 1 minute, and the percentage of CO_2 adsorbed at this stage respect to the total adsorbed after 6 minutes. All sorbents show relatively low selectivity, likely because of the more moderate textural properties that these sorbents possess (Manyà et al., 2018), compared to that of other sorbents reported in literature, as shown in Table 4. It is evident that all sorbents exhibit similar apparent selectivity, and that a slight increase was found on the activated samples compared to that of the carbonised sample. Minor variations were also observed within different burn-off values. These indicate a lower influence on the change in burn-off on the selectivity compared to the effect found on CO_2 adsorption capacity, where more notable changes were observed which may be attributed to all the sorbents already possessing similar, highly microporous structures. These selectivity values are also likely to be higher in multicomponent gaseous mixtures (Chao et al., 2021), hence further ratification of the selectivity estimates may be needed for these sorbents in flue gas representative mixtures.

3.9. Discussion

The experimental findings represent a promising initial step in the development of these sorbents for post combustion applications. These sorbents have shown promise in comparison to Norit R as a benchmark, meaning their performance warrants further comparative analysis with more commercially available sorbents designed for CO_2 capture. This expanded analysis will be more beneficial if conducted at larger scale experimental conditions that are more applicable to realistic post-combustion conditions.

This includes testing the sorbent CO_2 adsorption capacity in multi-component streams that mimic the compositions of the combustion streams, from which a more practical assessment of CO_2 selectivity can be made. As mentioned previously, CO_2 selectivity calculated for these sorbents could be considered as a moderate estimation of the true sorbent selectivity. However, guaranteeing higher CO_2 selectivities and the quality of the CO_2 capture performance in a scaled-up experimental process will largely depend on the influence of the scaled-up operating conditions. Ensuring that a favourable influence (maximised CO_2 adsorption) on the sorbent performance is achieved requires adopting the appropriate TSA configuration for these sorbents. Configurations

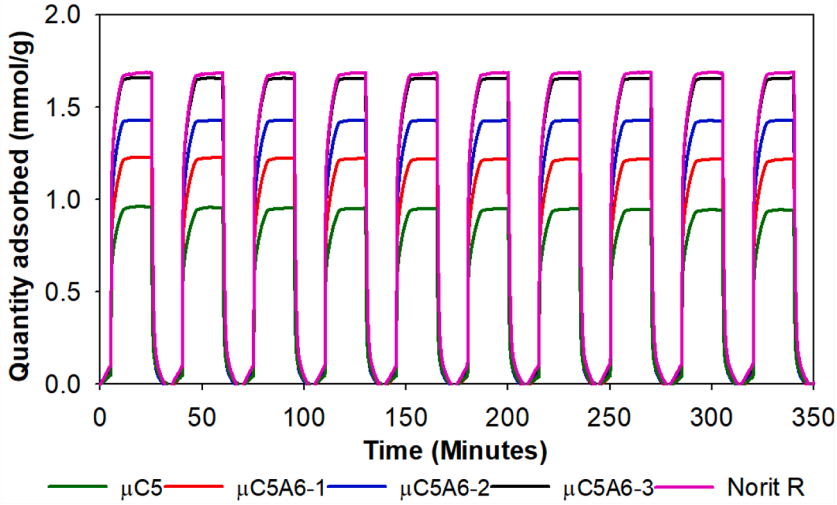

Fig. 9. MCC sorbents 10-Cycle CO_2 TGA adsorption-desorption profiles.

Table 6
CO_2/N_2 apparent selectivity at 25°C and 101.3 kPa, calculated from TGA adsorption experiments.

Sample	CO_2 adsorbed after 1 minute (mmol/g)	Percentage of CO_2 adsorbed (%)	Apparent selectivity (molar basis)
μC5	0.59	65.6	12.0
μC5A6-1	0.78	66.7	14.8
μC5A6-2	0.97	70.8	13.4
μC5A6-3	1.11	70.3	14.5

that are typically considered for TSA applications are fixed, fluidised bed, moving and rotating bed configurations (Dhoke et al., 2021). The fixed bed configuration is considered less complex compared to the other configurations, making it an attractive option (Dhoke et al., 2021). However, key challenges associated with fixed bed configurations that will require addressing include low heat transfer rates, larger energy consumption, lower productivity and large heat exchange areas required (Zhao et al., 2019). Most notably, fine particle materials, such as these MCC-derived ACs, are not particularly suitable for fixed bed TSA configurations, due to the substantial pressure drops that would emerge during operation (Raganati et al., 2016). To resolve this issue, ACs can be converted to larger particle forms through pelletisation. Whilst possibly addressing the issue of substantial pressure drops, ACs in pellet form produce slower adsorption kinetics due to increased intraparticle diffusion resistance (Raganati et al., 2016). The physical changes to the sorbent that occur through pelletisation may also hinder sorbent textural properties and CO_2 capturing capability (Raganati et al., 2016). The extent of this hinderance would need to be assessed, likely through comparative study of the textural and adsorptive properties of the MCC-based ACs in fine particle and pellet form. In the event that the pelletisation process is too detrimental to the performance of these ACs or at least in fixed bed conditions, alternative, commercially-scalable configurations will need to be considered, such as those previously mentioned.

Regardless of the configuration selected, modelling of the adsorption and desorption kinetic performance of sorbents under these varied conditions will provide beneficial insights into their adsorption-desorption behaviour that will aid designing and simulating behaviour in larger scale experiments. Parameters for consideration upon scale up include the purity, recovery and working capacity (Yassin et al., 2021), which in their assessing will yield a closer reflection of the sorbent performance in post-combustion conditions. Nonetheless, in this work, considering the preliminarily promising cyclic stability of these MCC-based sorbents, it is clear that promise for their development and incorporation at larger experimental scales exists. This with the added benefit of a production procedure which lacks complexity compared to other novel AC production procedures, and with a promising degree of commercial feasibility, of course subject to further life cycle assessment and feasibility analysis.

4. Conclusions

This study investigated, for the first time, the production of activated carbons from microcrystalline cellulose, following a simple two-step physical activation procedure using moderate activation conditions for their incorporation into post-combustion CO_2 capture applications. Through the presented methods, raw microcrystalline cellulose was converted into promising sorbents for carbon capture, with well-defined critical characteristics for the sought-after application. This includes significant thermal stability, predominantly neutral surface character and a chemical structure consisting of substantial content of aromatic functional groups. The activated carbons produced with burn-offs of 10, 20 and 30% showed to be largely microporous. Whilst microporosity ratios within all sorbents remained the same, an increase in burn-off resulted in increased pore volumes, especially in the region of the ultramicropores, and narrower pore sizes, which ultimately proved beneficial for CO_2 adsorption. This is the case of the activated carbon produced with 30% burn-off, which exhibited the highest CO_2 capture capacity. The capture capacities revealed to be suitable and comparable to those of other LCB-based sorbents, however it is the abundance of MCC in various waste forms which also provides an advantage for MCC-based sorbents.. Regarding characterisation of the sorbent surface, point of zero charge results indicated a near-neutral surface character across all sorbents, whilst heat of adsorption calculations not only confirmed that there is substantial adsorption affinity between CO_2 and the surface of the ACs, but also a heterogeneous surface. In addition, the demonstrated thermal stability, and the capture stability over 10 adsorption/desorption cycles, proved these sorbents as favourable for CO_2 capture cyclic processes. Finally, the 30% burn-off AC showed similar, comparable cyclic CO_2 capture capacity when compared to a commercially available CO_2-capturing sorbent (Norit R). The findings of this work can serve as a premise incorporation of these sorbents in larger TSA experimental processes that can test larger quantities of sorbents, this of course subject to the appropriate bed configuration adopted. In addition, the simplicity and scalability of the production process, performed at conditions considered moderate for physical activation, suggest a more

scalable, more environmentally feasible production process compared to other Novel AC production routes.

Finally, considering the promising findings presented in this work, taking into account the environmental benefits of using MCC as feedstock, its abundance, there is a clear justification for progressing with the use of MCC-based ACs to improve the sustainability of post-combustion carbon capture.

Declaration of competing interest

The authors declare that they have no known competing financial interests or personal relationships that could have appeared to influence the work reported in this paper.

Data availability

No data was used for the research described in the article.

Acknowledgements

Authors would like to thank The Leverhulme Trust for the funding provided through the Grant DS-2017-073. Simbarashe Biti, a Leverhulme Trust Doctoral Scholar, is part of the 15 PhD scholarships of the 'Leverhulme Centre for Doctoral Training in Sustainable Production of Chemicals and Materials' at the University of Aberdeen (Scotland, United Kingdom). Surface morphology data was completed with the assistance of the ACEMAC SEM facility at the University of Aberdeen. Elemental analysis data was produced with the assistance of the Analytical Facilities in the School of Chemistry at the University of Birmingham.

References

Abd, A.A., Naji, S.Z., Hashim, A.S., Othman, M.R., 2020. Carbon dioxide removal through physical adsorption using carbonaceous and non-carbonaceous adsorbents: a review. J. Environ. Chem. Eng. 8, 104142 https://doi.org/10.1016/J.JECE.2020.104142.

Abdullah, M.Z., Qasim, A., 2016. Parametric analysis of carbon dioxide adsorption on nanoporous activated carbon using computational approach. Procedia Eng. C 1416–1422. https://doi.org/10.1016/J.PROENG.2016.06.626.

Abuelnoor, N., AlHajaj, A., Khaleel, M., Vega, L.F., Abu-Zahra, M.R.M., 2021. Activated carbons from biomass-based sources for CO2 capture applications. Chemosphere 282, 131111. https://doi.org/10.1016/J.CHEMOSPHERE.2021.131111.

Ahmed, M.B., Hasan Johir, M.A., Zhou, J.L., Ngo, H.H., Nghiem, L.D., Richardson, C., Moni, M.A., Bryant, M.R., 2019. Activated carbon preparation from biomass feedstock: clean production and carbon dioxide adsorption. J. Clean. Prod. 225, 405–413. https://doi.org/10.1016/J.JCLEPRO.2019.03.342.

Ammendola, P., Raganati, F., Chirone, R., 2017. CO2 adsorption on a fine activated carbon in a sound assisted fluidized bed: thermodynamics and kinetics. Chem. Eng. J. 322, 302–313. https://doi.org/10.1016/J.CEJ.2017.04.037.

E.S. Azzi, E. Karltun, C. Sundberg, Prospective life cycle assessment of large-scale biochar production and use for negative emissions in Stockholm, (2019). https://doi.org/10.1021/acs.est.9b01615.

Bernal, V., Giraldo, L., Moreno-Piraján, J., 2018. Physicochemical properties of activated carbon: their effect on the adsorption of pharmaceutical compounds and adsorbate–adsorbent interactions. C (Basel). 4, 62. https://doi.org/10.3390/c4040062.

Bezerra, D.P., Oliveira, R.S., Vieira, R.S., Cavalcante, C.L., Azevedo, D.C.S., 2011. Adsorption of CO2 on nitrogen-enriched activated carbon and zeolite 13X. Adsorption 17 (1), 235–246. https://doi.org/10.1007/S10450-011-9320-Z, 201117.

Chao, C., Deng, Y., Dewil, R., Baeyens, J., Fan, X., 2021. Post-combustion carbon capture. Renew. Sustainable Energy Rev. 138 https://doi.org/10.1016/J.RSER.2020.110490.

Cheng, F., Luo, H., Colosi, L.M., 2020. Slow pyrolysis as a platform for negative emissions technology: An integration of machine learning models, life cycle assessment, and economic analysis. Energy Convers. Manag. 223, 113258 https://doi.org/10.1016/J.ENCONMAN.2020.113258.

Choi, S., Gray, M.L., Jones, C.W., 2011. Amine-tethered solid adsorbents coupling high adsorption capacity and regenerability for CO2 capture from ambient air. ChemSusChem 4, 628–635. https://doi.org/10.1002/CSSC.201000355.

Chowdhury, S., Mishra, R., Saha, P., Kushwaha, P., 2011. Adsorption thermodynamics, kinetics and isosteric heat of adsorption of malachite green onto chemically modified rice husk. Desalination 265, 159–168. https://doi.org/10.1016/j.desal.2010.07.047.

N.B. Colthup, Introduction to infrared and Raman spectroscopy Norman B. Colthup, Lawrence H. Daly, Stephen E. Wiberley., (1990) 547.

Creamer, A.E., Gao, B., 2016. Carbon-based adsorbents for postcombustion CO2 capture: a critical review. Environ. Sci. Technol. 50, 7276–7289. https://doi.org/10.1021/ACS.EST.6B00627/ASSET/IMAGES/LARGE/ES-2016-00627A_0011.JPEG.

C. Dhoke, A. Zaabout, S. Cloete, S. Amini, Review on reactor configurations for adsorption-based CO 2 capture, (2021). https://doi.org/10.1021/acs.iecr.0c04547.

Garba, Z.N., Lawan, I., Zhou, W., Zhang, M., Wang, L., Yuan, Z., 2020. Microcrystalline cellulose (MCC) based materials as emerging adsorbents for the removal of dyes and heavy metals – a review. Sci. Total Environ. 717 https://doi.org/10.1016/J.SCITOTENV.2019.135070.

García-Freites, S., Gough, C., Röder, M., 2021. the greenhouse gas removal potential of bioenergy with carbon capture and storage (BECCS) to support the UK's net-zero emission target. Biomass Bioenergy 151, 106164. https://doi.org/10.1016/J.BIOMBIOE.2021.106164.

González, A.S., Plaza, M.G., Rubiera, F., Pevida, C., 2013. Sustainable biomass-based carbon adsorbents for post-combustion CO2 capture. Chem. Eng. J. 230, 456–465. https://doi.org/10.1016/j.cej.2013.06.118.

González, B., Manyà, J.J., 2020. Activated olive mill waste-based hydrochars as selective adsorbents for CO2 capture under postcombustion conditions. Chem. Eng. Processing - Process Intensification 149. https://doi.org/10.1016/J.CEP.2020.107830.

Greig, C., Uden, S., 2021. The value of CCUS in transitions to net-zero emissions. The Electricity J. 34, 107004 https://doi.org/10.1016/J.TEJ.2021.107004.

Guo, Y., Tan, C., Sun, J., Li, W., Zhang, J., Zhao, C., 2020. Porous activated carbons derived from waste sugarcane bagasse for CO2 adsorption. Chem. Eng. J. 381, 122736 https://doi.org/10.1016/j.cej.2019.122736.

Y. Guo, H. Zhang, Y. Liu, Desorption characteristics and kinetic parameters determination of molecular sieve by thermogravimetric analysis/differential thermogravimetric analysis technique,. 36 (2018) 1389–1404. https://doi.org/10.1177/0263617418772665.

Hedin, N., Andersson, L., Bergström, L., Yan, J., 2013. Adsorbents for the post-combustion capture of CO2 using rapid temperature swing or vacuum swing adsorption. Appl. Energy 104, 418–433. https://doi.org/10.1016/J.APENERGY.2012.11.034.

Heidari, A., Younesi, H., Rashidi, A., Ghoreyshi, A.A., 2014. Evaluation of CO2 adsorption with eucalyptus wood based activated carbon modified by ammonia solution through heat treatment. Chem. Eng. J. 254, 503–513. https://doi.org/10.1016/j.cej.2014.06.004.

Joseph, C.G., Quek, K.S., Daud, W.M.A.W., Moh, P.Y., 2017. Physical activation of oil palm empty fruit bunch via co2 activation gas for CO2 adsorption. In: IOP Conf Ser Mater Sci Eng. Institute of Physics Publishing, 012003. https://doi.org/10.1088/1757-899X/206/1/012003.

Kassanov, B., Wang, J., Fu, Y., Chang, J., 2017. Cellulose enzymatic saccharification and preparation of 5-hydroxymethylfurfural based on bamboo hydrolysis residue separation in ionic liquids. RSC Adv. 7, 30755–30762. https://doi.org/10.1039/C7RA05020H.

Kian, L.K., Jawaid, M., Ariffin, H., Alothman, O.Y., 2017. Isolation and characterization of microcrystalline cellulose from roselle fibers. Int. J. Biol. Macromol. 103, 931–940. https://doi.org/10.1016/J.IJBIOMAC.2017.05.135.

A.H. Lahuri, R. Adnan, N. Nordin, Adsorption kinetics for carbon dioxide capture using bismuth(III) oxide impregnated on activated carbon †, (n.d.). https://www.researchgate.net/publication/340827733 (accessed August 9, 2022).

Li, M., Xiao, R., 2019. Preparation of a dual pore structure activated carbon from rice husk char as an adsorbent for CO2 capture. Fuel Processing Technol. 186, 35–39. https://doi.org/10.1016/J.FUPROC.2018.12.015.

Ma, C., Bai, J., Demir, M., Hu, X., Liu, S., Wang, L., 2022. Water chestnut shell-derived N/S-doped porous carbons and their applications in CO2 adsorption and supercapacitor. Fuel 326, 125119. https://doi.org/10.1016/J.FUEL.2022.125119.

Malini, K., Selvakumar, D., Kumar, N.S., 2023. Activated carbon from biomass: Preparation, factors improving basicity and surface properties for enhanced CO2 capture capacity – A review. J. CO2 Utilization 67, 102318. https://doi.org/10.1016/J.JCOU.2022.102318.

Manyà, J.J., González, B., Azuara, M., Arner, G., 2018. Ultra-microporous adsorbents prepared from vine shoots-derived biochar with high CO2 uptake and CO2/N2 selectivity. Chem. Eng. J. 345, 631–639. https://doi.org/10.1016/j.cej.2018.01.092.

Martín, C.F., Plaza, M.G., García, S., Pis, J.J., Rubiera, F., Pevida, C., 2011. Microporous phenol–formaldehyde resin-based adsorbents for pre-combustion CO2 capture. Fuel 90, 2064–2072. https://doi.org/10.1016/J.FUEL.2011.01.019.

Martín, C.F., Plaza, M.G., Pis, J.J., Rubiera, F., Pevida, C., Centeno, T.A., 2010. On the limits of CO2 capture capacity of carbons. Sep. Purif. Technol. 74, 225–229. https://doi.org/10.1016/J.SEPPUR.2010.06.009.

Martín, C.F., Stöckel, E., Clowes, R., Adams, D.J., Cooper, A.I., Pis, J.J., Rubiera, F., Pevida, C., 2011. Hypercrosslinked organic polymer networks as potential adsorbents for pre-combustion CO2 capture. J. Mater. Chem. 21, 5475–5483. https://doi.org/10.1039/C0JM03534C.

Masson-Delmotte, V., Zhai, P., Pirani, A., Connors, S.L., Péan, C., Berger, S., Caud, N., Chen, Y., Goldfarb, L., Gomis, M.I., Huang, M., Leitzell, K., Lonnoy, E., Matthews, J. B.R., Maycock, T.K., Waterfield, T., Yelekçi, O., Yu, R., Zhou, B., 2021. Contribution of Working Group I to the Sixth Assessment Report of the Intergovernmental Panel on Climate Change. https://www.ipcc.ch/report/ar6/wg1/ (accessed February 11, 2022).

Mukherjee, A., Okolie, J.A., Abdelrasoul, A., Niu, C., Dalai, A.K., 2019. Review of post-combustion carbon dioxide capture technologies using activated carbon. J. Environ. Sci. 83, 46–63. https://doi.org/10.1016/J.JES.2019.03.014.

Noh, J.S., Schwarz, J.A., 1989. Estimation of the point of zero charge of simple oxides by mass titration. J. Colloid Interface Sci. 130, 157–164. https://doi.org/10.1016/0021-9797(89)90086-6.

Plaza, M.G., García, S., Rubiera, F., Pis, J.J., Pevida, C., 2010. Post-combustion CO2 capture with a commercial activated carbon: Comparison of different regeneration strategies. Chem. Eng. J. 163, 41–47. https://doi.org/10.1016/J.CEJ.2010.07.030.

Plaza, M.G., González, A.S., Pis, J.J., Rubiera, F., Pevida, C., 2014. Production of microporous biochars by single-step oxidation: effect of activation conditions on CO2 capture. Appl. Energy 114, 551–562. https://doi.org/10.1016/J.APENERGY.2013.09.058.

Quan, C., Jia, X., Gao, N., 2020. Nitrogen-doping activated biomass carbon from tea seed shell for CO2 capture and supercapacitor. Int. J. Energy Res. 44, 1218–1232. https://doi.org/10.1002/ER.5017.

C. Quan, R. Su, N. Gao, Preparation of activated biomass carbon from pine sawdust for supercapacitor and CO 2 capture, (2020). https://doi.org/10.1002/er.5206.

Raganati, F., Ammendola, P., Chirone, R., 2016. On improving the CO2 recovery efficiency of a conventional TSA process in a sound assisted fluidized bed by separating heating and purging. Sep. Purif. Technol. 167, 24–31. https://doi.org/10.1016/J.SEPPUR.2016.05.001.

Raganati, F., Chirone, R., Ammendola, P., 2020. CO2 capture by temperature swing adsorption: working capacity as affected by temperature and CO2 partial pressure. Ind. Eng. Chem. Res. 59, 3593–3605. https://doi.org/10.1021/ACS.IECR.9B04901/ASSET/IMAGES/LARGE/IE9B04901_0006.JPEG.

F. Raganati, F. Miccio, P. Ammendola, Adsorption of carbon dioxide for post-combustion capture: a review, (2021). https://doi.org/10.1021/acs.energyfuels.1c01618.

Ramos, P.B., Ponce, M.F., Jerez, F., Barreto, G.P., Bavio, M.A., 2022. Assessment of industrial waste for adsorption and capture of CO2: Dynamic and static capture system. J. Environ. Chem. Eng. 10, 107521 https://doi.org/10.1016/J.JECE.2022.107521.

Rao, N., Wang, M., Shang, Z., Hou, Y., Fan, G., Li, J., 2018. CO2 adsorption by amine-functionalized MCM-41: a comparison between impregnation and grafting modification methods. Energy and Fuels 32, 670–677. https://doi.org/10.1021/ACS.ENERGYFUELS.7B02906/ASSET/IMAGES/LARGE/EF-2017-02906H_0010.JPEG.

Rashidi, N.A., Yusup, S., 2016. An overview of activated carbons utilization for the post-combustion carbon dioxide capture. J. CO2 Utilization. https://doi.org/10.1016/j.jcou.2015.11.002.

Rashidi, N.A., Yusup, S., 2017. Potential of palm kernel shell as activated carbon precursors through single stage activation technique for carbon dioxide adsorption. J. Clean. Prod. 168, 474–486. https://doi.org/10.1016/J.JCLEPRO.2017.09.045.

Rehman, A., Nazir, G., Yop Rhee, K., Park, S.-J., 2021. A rational design of cellulose-based heteroatom-doped porous carbons: promising contenders for CO2 adsorption and separation. Chem. Eng. J. 420, 130421 https://doi.org/10.1016/j.cej.2021.130421.

Serafin, J., Narkiewicz, U., Morawski, A.W., Wróbel, R.J., Michalkiewicz, B., 2017. Highly microporous activated carbons from biomass for CO2 capture and effective micropores at different conditions. J. CO2 Utilization 18, 73–79. https://doi.org/10.1016/J.JCOU.2017.01.006.

Sethia, G., Sayari, A., 2015. Comprehensive study of ultra-microporous nitrogen-doped activated carbon for CO2 capture. Carbon N Y 93, 68–80. https://doi.org/10.1016/j.carbon.2015.05.017.

Sha, Y., Lou, J., Bai, S., Wu, D., Liu, B., Ling, Y., 2015. Facile preparation of nitrogen-doped porous carbon from waste tobacco by a simple pre-treatment process and their application in electrochemical capacitor and CO2 capture. Mater. Res. Bull. 64, 327–332. https://doi.org/10.1016/j.materresbull.2015.01.015.

Suhas, V.K.Gupta, Carrott, P.J.M., Singh, R., Chaudhary, M., Kushwaha, S., 2016. Cellulose: A review as natural, modified and activated carbon adsorbent. Bioresour. Technol. 216, 1066–1076. https://doi.org/10.1016/j.biortech.2016.05.106.

Trache, D., Donnot, A., Khimeche, K., Benelmir, R., Brosse, N., 2014. Physico-chemical properties and thermal stability of microcrystalline cellulose isolated from Alfa fibres. Carbohydr. Polym. 104, 223–230. https://doi.org/10.1016/J.CARBPOL.2014.01.058.

Trache, D., Hussin, M.H., Hui Chuin, C.T., Sabar, S., Fazita, M.R.N., Taiwo, O.F.A., Hassan, T.M., Haafiz, M.K.M., 2016. Microcrystalline cellulose: Isolation, characterization and bio-composites application—A review. Int. J. Biol. Macromol. 93, 789–804. https://doi.org/10.1016/j.ijbiomac.2016.09.056.

Vargas, D.P., Giraldo, L., Silvestre-Albero, J., Moreno-Piraján, J.C., 2011. CO2 adsorption on binderless activated carbon monoliths. Adsorption 17, 497–504. https://doi.org/10.1007/s10450-010-9309-z.

Xin, S., Yang, H., Chen, Y., Yang, M., Chen, L., Wang, X., Chen, H., 2015. Chemical structure evolution of char during the pyrolysis of cellulose. J. Anal. Appl. Pyrolysis 116, 263–271. https://doi.org/10.1016/J.JAAP.2015.09.002.

Xu, C., Ruan, C.Q., Li, Y., Lindh, J., Strømme, M., 2018. High-performance activated carbons synthesized from nanocellulose for CO2 capture and extremely selective removal of volatile organic compounds. Adv. Sustain. Syst. 2 https://doi.org/10.1002/ADSU.201700147.

Yassin, M.M., Anderson, J.A., Dimitrakis, G.A., Martín, C.F., 2021. Effects of the heating source on the regeneration performance of different adsorbents under post-combustion carbon capture cyclic operations. A comparative analysis. Sep. Purif. Technol. 276, 119326 https://doi.org/10.1016/J.SEPPUR.2021.119326.

Yassin, M.M., Biti, S., Afzal, W., Fernández Martín, C., 2021. A systematic analysis of the dynamics of microwave- and conventionally-assisted swing adsorption on zeolite 13X and an activated carbon under post-combustion carbon capture conditions. J. Environ. Chem. Eng. 9, 106835 https://doi.org/10.1016/J.JECE.2021.106835.

F. Zerobin, T. Prö, Concentrated carbon dioxide (CO 2) from diluted sources through continuous temperature swing adsorption (TSA), (2020). https://doi.org/10.1021/acs.iecr.9b06177.

Zhang, C., Chao, L., Zhang, Z., Zhang, L., Li, Q., Fan, H., Zhang, S., Liu, Q., Qiao, Y., Tian, Y., Wang, Y., Hu, X., 2021. Pyrolysis of cellulose: evolution of functionalities and structure of bio-char versus temperature. Renew. Sustainable Energy Rev. 135, 110416 https://doi.org/10.1016/J.RSER.2020.110416.

Zhao, R., Liu, L., Zhao, L., Deng, S., Li, S., Zhang, Y., 2019. A comprehensive performance evaluation of temperature swing adsorption for post-combustion carbon dioxide capture. Renew. Sustainable Energy Rev. 114, 109285 https://doi.org/10.1016/J.RSER.2019.109285.